# Geometric Basis of Entanglement in Six-Dimensional Space-Time

Seyed Kazem Mousavi * and Elham Razzazi

Posted Date: 15 May 2025

doi: 10.20944/preprints202505.1200.v1

Keywords: Prime Numbers; Six-Dimensional Space-Time; Quantum Entanglement; Möbius Geometry; Bell's Inequality Violation; Geometric Throats; Wormhole Constriction Points; Density Fluctuations; Internal Digit Sum (INDS); Quantum Information

 doi:10.20944/preprints202505.1200.v1



*Article*

# Geometric Basis of Entanglement in Six-Dimensional Space-Time

**Seyed Kazem Mousavi * and Elham Razzazi**

Independent Researcher

* Correspondence: Mousavi1142@iran.ir/+989140765784

**Abstract:** This paper proposes a framework uniting prime number distribution, six-dimensional spacetime structure, and quantum entanglement. By utilizing Internal Digit Sum (INDS) classification, we show that prime numbers distribute into six residue classes modulo nine, with classes 3, 6, and 9 notably absent of primes, except for 3. Prime gaps reveal geometric features that align with density fluctuations in a Möbius-like six-dimensional spacetime. These features connect the laws of wormholes and entanglement through the geometric Constriction Points of Möbius space. The violation of Bell's inequality results from the existence of two orthogonal time dimensions. The algebraic structure governing primes underpins both quantum information and spacetime geometry. The entanglement phenomenon arises from these algebraic relations, with implications for quantum mechanics and spacetime dynamics.

**Keywords:** prime numbers; six-dimensional space-time; quantum entanglement; Möbius geometry; Bell's inequality violation; geometric throats; wormhole Constriction points; density fluctuations; internal digit sum (INDS); quantum information

## 1. Introduction

The violation of Bell's inequality constitutes the foundation of the phenomenon of entanglement, which establishes a direct connection with the structure of space-time. [1] Information is the basis for the existence of natural facts on the algebraic platform of mathematics, and mathematics is the differentiable algebraic field governing numbers. [2] The structure of the universe cannot adopt a dual approach to natural phenomena within a single algebraic field. [3] Based on this, the connection between quantum mechanical phenomena and classical events is entirely embedded in the fundamental informational structure of the universe that is, numbers. [4] And the structure of numbers is also enclosed in geometry. [5] The structure of number fields is both embedded and enclosed in geometry. Therefore, the geometric expression of information related to both macroscopic and microscopic phenomena depends on the specific distribution of numbers based on the geometry of space-time. [6] The progression of time and the transformation of governing algebraic environments reveal an intrinsic connection between numbers and geometry. A six-dimensional space-time framework provides a coherent model for describing the underlying relationship between geometry and the temporal dimension. [7] In this work, we examine quantum entanglement through this theoretical lens and formulate a geometric interpretation of the relationship between the distribution of prime numbers and the violation of Bell's inequality. Based on empirical observations, we explore the possibility of instantaneous transmission and decoding of compressed quantum information, along with the breakdown of specific proportional relations. [8][9] Trigonometric ratios allow for the classification of all numbers into sets sharing identical properties. Accordingly, by applying internal digit sum (INDS) classification, numbers are divided into six modular groups, where prime numbers are numerical absent from groups 3, 6, and 9, except for the prime 3 itself. Furthermore, prime gaps within these six groups show an approximation-regular recurrence, where the resulting gaps oscillate across rows and columns. Oscillations also occur in geometric structures. Ratios associated with the golden ratio and Euler's number generate geometric oscillations in the

 doi:10.20944/preprints202505.1200.v1



structure of space-time. Time results from a geometric potential difference produced by oscillations and tension in matter and energy across different dimensions. [10] The Möbius geometry transfers the properties of lower dimensions to higher dimensions and vice versa, and the change in geometric pressure caused by tension at the throats of Möbius space expresses the geometric form of Bernoulli's principle, which is directly related to the gaps between prime numbers in different groups. Furthermore, the loops in the structure of space-time result from the intrinsic expansion of space across dimensions. This expansion gives rise to recurrent oscillatory states in the wave function. Accordingly, Hilbert space arises from the temporal repetition of these oscillation states. Accordingly, within this framework, entanglement is defined through the geometry of prime number groups in space-time, via the violation of Bell's inequality allowing for the control and directed transmission of information through entanglement. [9]

## 2. Methodology

Locality and realism are functions of the geometric structure of space-time. Accordingly, the correlation function is defined based on density fluctuations along the time vector. Within this framework, identical particle densities are effective in generating quantum entanglement. The violation of Bell's inequality represents a correlation between geometric potential differences over time (2.1). Therefore, a new formulation of Bell's inequality can be expressed as a function of time. The wave function consists of small packets embedded in phase space, and matter and energy are embedded in the real dimension of time (temporal dimension). The absence of mass in the past and future is defined by negative density (2.1). Mass and energy cause geometric changes in the structure of space and time. The potential difference resulting from the absence of density in the past and future causes the movement of matter in the real dimension of time. This geometric potential difference is the driver of cosmic expansion. On this basis, the relation between density fluctuations and the wave function in the present depends on the small wave-function packets in phase space. The equivalence of density with changes in length and velocity over time gives rise to the matter-wave phenomenon (2.1).

$$A, B\epsilon\ \Psi_{\mu\upsilon} + G_{\mu\upsilon} + \Lambda_{g_{\mu\upsilon}} \qquad 2.1$$

$$\frac{\partial\rho}{\partial t} \equiv \frac{v}{c} \Rightarrow v = \frac{\partial x}{\partial t} \;\Rightarrow \left(\frac{\partial x_i}{c}\right) \equiv \partial\rho \quad i = 1,2,3 \;\; \sin\left(arccos\left(\frac{\partial x_i}{c}\right)\right) = \sqrt{1-(\partial\rho)^2}$$

$$-\rho \in t_-, t_+ \quad \rho \in t \qquad \longrightarrow \psi = \sqrt{\rho}.e^{-i\gamma}$$

$$\int_{-\rho}^{+\rho}\int_{-t}^{+t}\int_{-\infty}^{+\infty} |\psi(\rho,t,x)|^2 d\rho dt dx = 1 \quad ,$$

$$|\Psi\rangle = b_1|\tilde{\psi}_1\rangle + b_2|\tilde{\psi}_2\rangle + \cdots + b_n|\tilde{\psi}_n\rangle$$
$$|\tilde{\psi}\rangle = \alpha_1|A_1\rangle + \alpha_2|A_2\rangle + \alpha_3|A_3\rangle + \alpha_4|A_4\rangle + \alpha_5|A_5\rangle + \alpha_6|A_6\rangle$$

$$b_\mu = x_\mu + ti \;, \quad X_\mu = (x_1, x_2, x_3, x_4, x_5, x_6) \Rightarrow b_\mu {b_\mu}^* = (\tfrac{1}{3})$$

$$\int_0^{2\pi}|\psi(x,t))|^2 dx = 1 \rightarrow \frac{2\pi}{6} \Longrightarrow \left\{\left(\frac{\pi}{3}\right) + i\left(\frac{2\pi}{3}\right)\right\}, \left\{\left(\frac{2\pi}{3}\right) + i\left(\frac{4\pi}{3}\right)\right\}, \{(\pi) + (i)\}, \left\{\left(\frac{4\pi}{3}\right) + i\left(\frac{5\pi}{3}\right)\right\}, \left\{\left(\frac{5\pi}{3}\right) + i(1)\right\}, \{(2\pi) + i(2\pi)\}$$

$$A_1 = \pm\left(\frac{\pi}{3}\right) + iz, A_2 = \pm\left(\frac{2\pi}{3}\right) + iz,\ A_3 = \pm(\pi) + iz\ , A_4 = \pm\left(\frac{4\pi}{3}\right) + iz,\ A_5 = \pm\left(\frac{5\pi}{3}\right) + iz, A_6 = \pm(2\pi) + iz,$$

 doi:10.20944/preprints202505.1200.v1



$$\sigma = 1,2,3,4,5,6$$

$$\Longrightarrow E(a,b) = \int_{-\rho}^{+\rho}\int_{-t}^{+t}\int_{-\infty}^{+\infty} |\psi(\rho,t,x)|^2 d\rho dt dx \tilde{\psi}(t_1, a\rho)\tilde{\psi}^{-1}(t_2, b\rho)$$

$$|00\rangle = \begin{bmatrix}1\\0\\0\\0\\0\\0\end{bmatrix}, |01\rangle = \begin{bmatrix}0\\1\\0\\0\\0\\0\end{bmatrix} |10\rangle = \begin{bmatrix}0\\0\\1\\0\\0\\0\end{bmatrix}, |11\rangle = \begin{bmatrix}0\\0\\0\\1\\0\\0\end{bmatrix}, |-+\rangle = \begin{bmatrix}0\\0\\0\\0\\1\\0\end{bmatrix}, |--\rangle = \begin{bmatrix}0\\0\\0\\0\\0\\1\end{bmatrix} \qquad 2.1$$

$$\left|\tilde{\psi}\right\rangle = \frac{1}{\sqrt{2}}(|01\rangle|10\rangle|--\rangle + |10\rangle|01\rangle|+-\rangle)$$

$$\left|\tilde{\psi}\right\rangle^{-1} = \frac{1}{\sqrt{2}}(|01\rangle|10\rangle|-+\rangle + |10\rangle|01\rangle|--\rangle)$$

$$\left|\acute{\Psi}\right\rangle = \frac{1}{\sqrt{2}}(|01\rangle|10\rangle|--\rangle + |10\rangle|01\rangle|-+\rangle) \quad \left\langle\acute{\Psi}\right| = \frac{1}{2}\left(\langle 01|\langle 10|\langle +-| + \langle 01|\langle 10|\langle --|\right)$$

$$|\Psi\rangle = \frac{1}{2\sqrt{2}}(|01\rangle_{\tilde{\psi}}|00\rangle_{\tilde{\psi}^{-1}} + |10\rangle_{\tilde{\psi}^{-1}}|00\rangle_{\tilde{\psi}} \otimes |01\rangle_{\tilde{\psi}^{-1}}|00\rangle_{\tilde{\psi}} + |10\rangle_{\tilde{\psi}}|00\rangle_{\tilde{\psi}^{-1}})$$

$$\sin 0 = 0 \Rightarrow x, t \neq c \quad \xi = \sin\left(\cos^{-1}\left(\frac{\Delta x}{c}\right)\right) + sin\left(cos^{-1}\left(\frac{\Delta y}{c}\right)\right) + sin\left(cos^{-1}\left(\frac{\Delta z}{c}\right)\right)$$

$$t = \frac{t_0}{\xi} \equiv t = t_0\sqrt{1 - \frac{2GM}{rc^2}} \Rightarrow c\left(\eta^2{}_1 + \eta^2{}_2 + \eta^2{}_3\right) = r_{x,\rho}c \Rightarrow \sin\left(\cos^{-1}\left(\frac{\sqrt{2GM}}{c\sqrt{r}}\right)\right) \equiv sin\phi$$

$$t = \frac{t_0}{\eta}\ ,\ l = \frac{l_0}{\eta}\ ,\ m = \frac{m_0}{\eta} \quad m^t = \frac{h\nu}{c^2}\ ,(\ \rho c)^{\frac{1}{2}} = \Delta\acute{x}\ , r_{x,\rho} = \Delta x + \Delta\acute{x}\ , \qquad 2.1$$

$$(m^t + m_x) = \frac{m^t}{\eta} \ \rightarrow sin\theta = \frac{m^t}{m^t + m_x}$$

$$(\rho c) = \Delta\acute{x}^2\ , \qquad \left(\frac{c}{\rho}\right) = \Delta\acute{t}^2$$

$$\rho = \left(\frac{m^t}{2\pi^2 r^3}\right)\ , m/\rho = \frac{2\pi^2 r^3}{\eta}$$

$$T_{\mu\nu} = \begin{bmatrix}-\rho^\dagger & 0 & 0 & 0 & 0 & 0\\ 0 & -\rho & 0 & 0 & 0 & 0\\ 0 & 0 & \rho & 0 & 0 & 0\\ 0 & 0 & 0 & P & 0 & 0\\ 0 & 0 & 0 & 0 & P & 0\\ 0 & 0 & 0 & 0 & 0 & P\end{bmatrix} \qquad \rho = \begin{bmatrix}\rho_{xx} & \rho_{xy} & \rho_{xz}\\ \rho_{yx} & \rho_{yy} & \rho_{yz}\\ \rho_{zx} & \rho_{zy} & \rho_{zz}\end{bmatrix}$$

$$\left|\left(\tilde{\psi}^2, \rho a\right) + \left(\tilde{\psi}^2, \rho b\right) + \left(\tilde{\psi}^2, -\rho a\right) + \left(\tilde{\psi}^2, -\rho b\right) + \left(\tilde{\psi}^2, -\rho^\dagger b\right) + \left(\tilde{\psi}^2, -\rho^\dagger a\right)\right| = 2\sqrt{2} \pm iP$$

$$\left\langle\tilde{\psi}\middle|\tilde{\psi}\right\rangle = \tilde{\psi}^2 \qquad \alpha_1{}^* = \sec\left(\arcsin\left(\log_c\left(\frac{\partial x}{\partial t}\right)\right)\right) = \frac{1}{\sqrt{1 - \frac{\left(ln\left(\frac{\partial x}{\partial t}\right)\right)^2}{(ln(c))^2}}}$$

$$\alpha_1 = \frac{1}{\sqrt{1 + \frac{\left(ln\left(\frac{\partial x}{\partial t}\right)\right)^2}{(ln(c))^2}}} \qquad \alpha_1{}^*\alpha_1 = (t,\rho),(t,-\rho)$$

 doi:10.20944/preprints202505.1200.v1



In Euclidean space-time, complex space is embedded within a higher-dimensional Euclidean framework. Expansion can generate the arrow of time. The real dimension of time, from the perspective of three-dimensional space, appears imaginary. Density fluctuations in Minkowski space-time correlate over time through rotation and divergence along the real time dimension. **Figure 1**

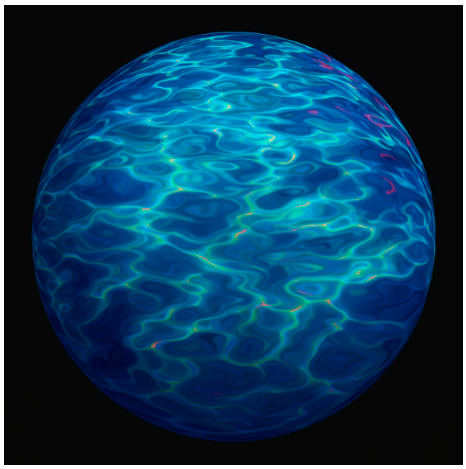

**Figure 1.** Locality and reality, through the oscillatory correlation of density variations over time, lead to the violation of Bell's inequality. Particles with identical density are embedded within a shared phase space in the present moment.

## 3. INDS

Using the Inner Digit Sum (INDS) method, prime numbers are divided into six groups with approximately regular intervals. Except for the prime number 3, no primes fall into groups 3, 6, or 9. Additionally, the INDS operation for multi-digit numbers may be repeated to yield a single-digit number corresponding to the properties of its group. (3.1) See **Table 1**.

$$INDS(P_\mu) = \lambda \epsilon G_\upsilon \qquad \upsilon = 1,2,4,5,7,8 \qquad 3.1$$

$$(INDS(\alpha\beta\gamma \dots \eta)) \Rightarrow INDS_n(n) = IDNS\left(INDS_{n-1}(n)\right) \ until \ \ INDS_n(n) \in \{1,2,,4,5,7,8\}$$

**Table 1.** Six group of prime numbers based on (INDS).

| 1 | 2 | 3 | 4 | 5 | 6 | 7 | 8 | 9 |
|---|---|---|---|---|---|---|---|---|
| 19 | 11 | | 13 | 23 | | 43 | 17 | |
| 37 | 29 | | 31 | 41 | | 61 | 53 | |
| 73 | 47 | | 67 | 59 | | 79 | 71 | |
| 109 | 83 | | 103 | 113 | | 97 | 89 | |
| 127 | 101 | | 139 | 131 | | 151 | 107 | |
| 163 | 137 | | 157 | 149 | | 223 | 179 | |
| 181 | 173 | | 193 | 167 | | 241 | 197 | |
| 199 | 191 | | 211 | 239 | | 277 | 233 | |
| 271 | 227 | | 229 | 257 | | 313 | 251 | |
| 307 | 263 | | 283 | 293 | | 331 | 269 | |
| 379 | 281 | | 337 | 311 | | 349 | 359 | |

 doi:10.20944/preprints202505.1200.v1



| | | | | | | | | |
|---|---|---|---|---|---|---|---|---|
| 397 | 317 | | 373 | 347 | | 367 | 431 | |
| 433 | 353 | | 409 | 383 | | | 449 | |

The spacing between numbers in each group is a multiple of 9. They also show the mathematical relationship between the rows and the momentary gaps of oscillatory behavior in the overall structure.

Each row is represented as a six-dimensional quantum state ket (3.2)

$$|\tilde{\psi}\rangle = \alpha_1|A_1\rangle + \alpha_2|A_2\rangle + \alpha_3|A_3\rangle + \alpha_4|A_4\rangle + \alpha_5|A_5\rangle + \alpha_6|A_6\rangle \qquad 3.2$$

Each oscillation period is modeled using a wave function (3.3)

$$|\Psi\rangle = b_1|\tilde{\psi}_1\rangle + b_2|\tilde{\psi}_2\rangle + \cdots + b_n|\tilde{\psi}_n\rangle \qquad 3.3$$

Given two orthogonal time axes, and based on the sum of the INDS of prime numbers, each group is assigned an angle in complex space. Additionally, the presence of weak correlations between rows and columns reflects the susceptibility of the geometric structure, the grouping of prime numbers in the hypergeometric distribution of mass, and other related correlations based on prime number groupings. (3.4)

$$sec^{-1}\left(2^{\alpha}2^{\beta}\ldots 2^{\eta}\right) = \theta \quad such \;\; 1777 \rightarrow sec^{-1}(2^1 2^7 2^7 2^7)$$

$$\boldsymbol{\alpha_1}|\boldsymbol{A_1}\rangle = 19 = \left(3\sqrt{2} + \left(\left(\sqrt{0}+1i\right)\left(\sqrt{0}-1i\right)\right)i\right)\left(3\sqrt{2} - \left(\left(\sqrt{0}+1i\right)\left(\sqrt{0}-1i\right)\right)i\right)$$

$$|\tilde{\psi}\rangle = \alpha_1|A_1\rangle + \alpha_2|A_2\rangle + \alpha_3|A_3\rangle + \alpha_4|A_4\rangle + \alpha_5|A_5\rangle + \alpha_6|A_6\rangle$$

$$\langle\widetilde{\psi_1}|\widetilde{\psi_1}\rangle = 19{,}11{,}13{,}23{,}43{,}17 = G_1$$

$$E\left(\Psi,\tilde{\psi}\right) = \int_0^{2\pi} \rho(P)\, A(\Psi,X) B(\tilde{\psi},Y) dP \qquad 3.4$$

$$\rho(P) \rightarrow \sum_{k=1}^{n} \left(\frac{x! + 2x!}{2}\right)^2 . \xi_n(P)$$

$$HG\rho(P) = \frac{\binom{4}{3}\binom{P_\mu - 4}{6-3}}{\binom{P_\mu}{6}}$$

Based on the intervals within each group shown in the table, the patterns associated with each group exhibit irregular oscillations. See Table 2

**Table 2.** The numerical gaps within each group exhibit an approximately uniform regularity.

| | **1** | **2** | **4** | **5** | **7** | **8** |
|---|---|---|---|---|---|---|
| **1 → 2** | 18 | 9 | 9 | 18 | 36 | 9 |
| **2 → 3** | 18 | 18 | 18 | 18 | 18 | 36 |
| **3 → 4** | 36 | 18 | 36 | 18 | 18 | 18 |
| **4 → 5** | 36 | 36 | 36 | 54 | 54 | 18 |
| **5 → 6** | 18 | 18 | 36 | 18 | 72 | 72 |
| **6 → 7** | 36 | 36 | 18 | 18 | 18 | 18 |

 doi:10.20944/preprints202505.1200.v1



| | | | | | | |
|---|---|---|---|---|---|---|
| **7 → 8** | 18 | 36 | 36 | 18 | 36 | 36 |
| **8 → 9** | 18 | 36 | 18 | 72 | 36 | 18 |
| **9 → 10** | 72 | 36 | 18 | 18 | 18 | 18 |
| **10 → 11** | 36 | 18 | 54 | 36 | 18 | 90 |
| **11 → 12** | 72 | 36 | 54 | 18 | 18 | 72 |
| **12 → 13** | 18 | 36 | 36 | 36 | 18 | |

Irregular oscillatory patterns can be observed in the gaps across the rows. See **Table 3**

**Table 3.** Compared to the columns, the number gaps across the rows display greater irregularity in their oscillatory patterns.

| **z** | | |
|---|---|---|
| **2** | 19, 11, 13, 23, 43, 17 | -8, 2, 10, 20, -26 |
| **3** | 37, 29, 31, 41, 61, 53 | -8, 2, 10, 20, -8 |
| **4** | 73, 47, 67, 59, 79, 71 | -26, 20, -8, 20, -8 |
| **5** | 109, 83, 103, 113, 97, 89 | -26, 20, 10, -16, -8 |
| **6** | 127, 101, 139, 131, 151, 107 | -26, 38, -8, 20, -44 |
| **7** | 163, 137, 157, 149, 223, 179 | -26, 20, -8, 74, -44 |
| **8** | 181, 173, 193, 167, 241, 197 | -8, 20, -26, 74, -44 |
| **9** | 199, 191, 211, 239, 277, 233 | -8, 20, 28, 38, -44 |
| **10** | 271, 227, 229, 257, 313, 251 | -44, 2, 28, 56, -62 |
| **11** | 307, 263, 283, 293, 331, 269 | -44, 20, 10, 38, -62 |
| **12** | 379, 281, 337, 311, 367, 431 | -98, 56, -26, 56, 64 |

The analysis of distance curves within each group describes the geometric structure of prime numbers, analogous to a spherical surface projected onto a two-dimensional plane. The observed gaps arise from the mismatch between spherical curvature and planar geometry. Figure 2

 doi:10.20944/preprints202505.1200.v1



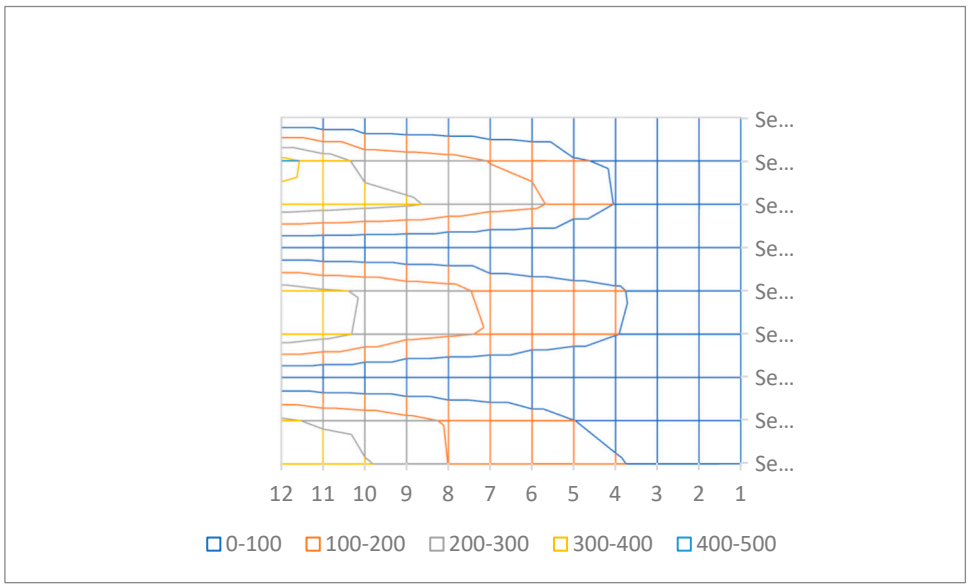


**Figure 2.** Irregular oscillations in the nearly regular gaps between prime numbers correspond to the geometric splitting of a spherical shell projected onto a two-dimensional plane.

The natural structures of prime number group intervals correlate with irregular geometric symmetries through oscillatory motion, and algebraic relationships also exist between the groups. Figures 3, 4, and 5.

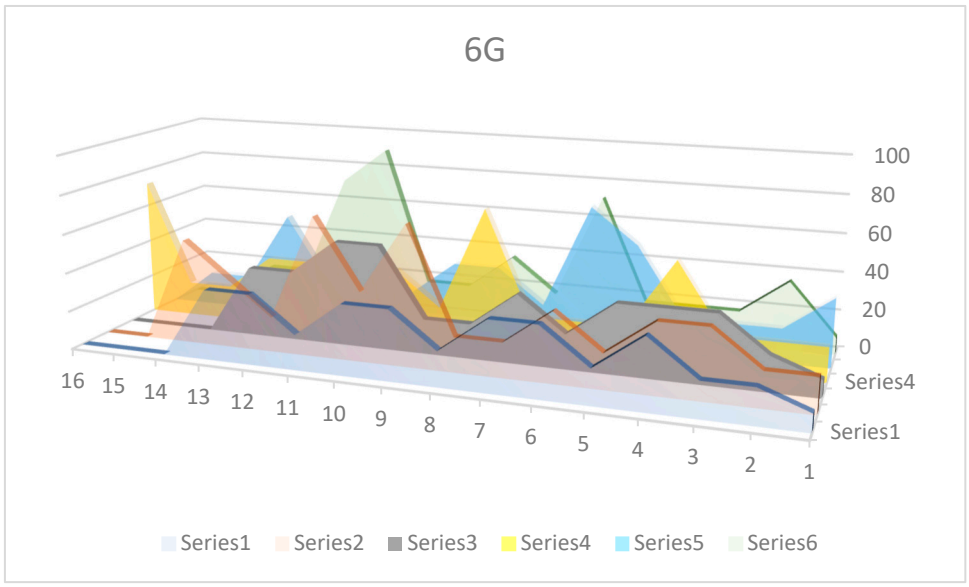


**Figure 3.**

Preprints.org (www.preprints.org) | NOT PEER-REVIEWED | Posted: 15 May 2025 doi:10.20944/preprints202505.1200.v1



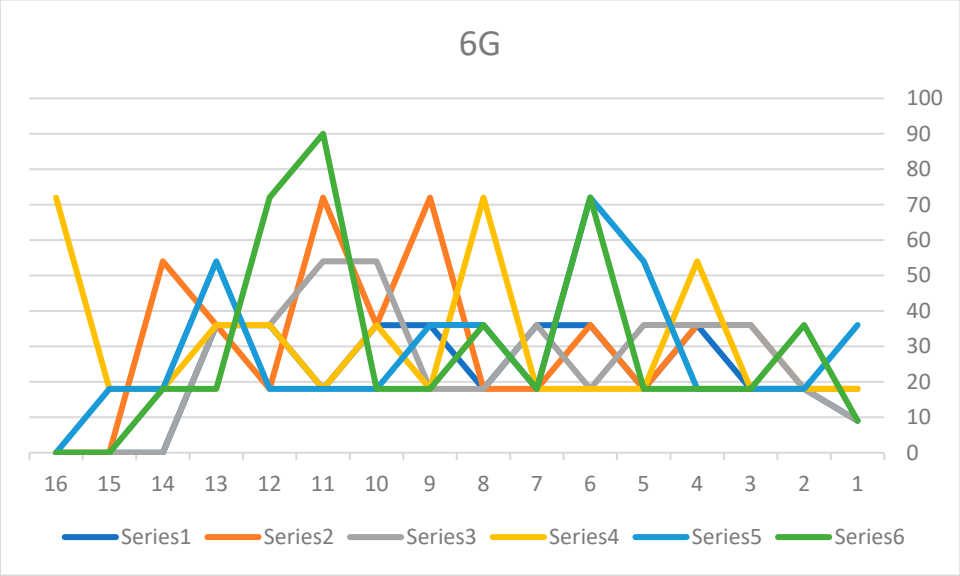


**Figure 4.** The weak correlation between rows and columns indicates the sensitivity of the geometric structure, the prime number groups within the hypergeometric distribution of mass, and other related correlations within the prime number group framework.

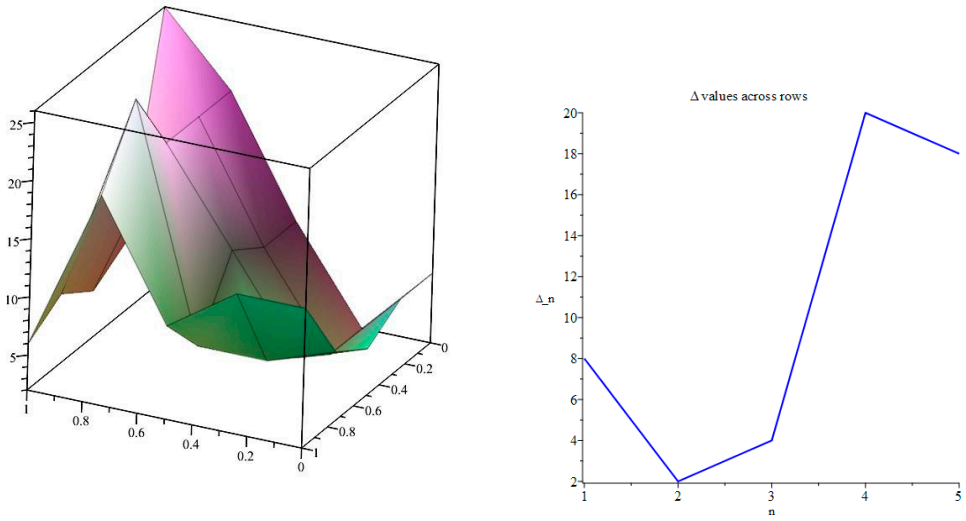


**Figure 5.**

The correlation function between rows and columns, along with the Fourier series, describes a dual oscillatory behavior. Each number is the product of two complex numbers; based on this, the correlation function is defined as continuous. (3.5)

$$E(\Psi,\tilde{\psi}) = \int_0^{2\pi} \rho(P)\, A(\Psi,X) B(\tilde{\psi},Y) dP$$

$$f(x) = a_0 + \sum_{n=1}^{\infty}\left( a_n\left(\cos\left(\frac{2\pi n x}{l}\right)\right) + b_n\left(\sin\left(\frac{2\pi n x}{l}\right)\right)\right) \qquad 3.5$$

$$a_0 = \frac{1}{l}\int_{-l}^{l} f(x)dx$$

$$a_n = \frac{1}{l}\int_{-l}^{l} f(x)\cos\left(\frac{2\pi n x}{l}\right)dx \qquad b_n = \frac{1}{l}\int_{-l}^{l} f(x)c\sin\left(\frac{2\pi n x}{l}\right)dx$$

 doi:10.20944/preprints202505.1200.v1



If each time an observer selects only three components from a row, and the second observer selects three components from a column, then the fourth number (complex) represents the joint wave function between the row and column components for both observers. The fourth number of the row observer becomes the fifth (complex) component of the column observer, and the fourth selection of the column observer becomes the fifth component of the row observer. Both the fourth and fifth components are imaginary. The only medium for mutual influence between the observers' selections is the imaginary dimension. More explicitly, entanglement is the component corresponding to interaction in the dimension of time. If each observer selects three spatial components either from a row or a column, then an imaginary fourth component emerges, not directly selected but determined by the entangled wave interaction. (3.6)

$$A(x,y,z) + \left(a\sqrt{2} + \left(\left(\sqrt{n} + it_1\right)\left(\sqrt{n} - it_1\right)\right) it_2\right)$$

$$B(x,y,z) + \left(a\sqrt{2} - \left(\left(\sqrt{n} + it_2\right)\left(\sqrt{n} - it_2\right)\right) it_1\right) \qquad (3.6)$$

$$|\Psi\rangle = \frac{1}{\sqrt{2}}(|01\rangle + |10\rangle)$$

$$\Psi\left(A_i, B_j, t\right) = \sum_{n=1}^{3}\sum_{m=1}^{3} c_{nm}\,(t)\Psi_n^{(A)}(x_n, t)\otimes\Psi_m^{(B)}(y_m, -t)$$

Two imaginary components, $t_1$ and $t_2$, respectively belong to the selections of Alice and Bob. The binary entanglement of selections in reciprocal terms results from position-dependent choices across two real dimensions of time. From the perspective of four-dimensional space, the joint wave function, structured as a seesaw function (a rotationally symmetric interference function) defined by an inverse relationship between eccentricity and centrality, places both imaginary dimensions along a single axis. The joint wave function overlaps with a seesaw function (**Figure 6**). The seesaw function depends on the eccentricity and the centrality of the ellipse. The eccentricity of the ellipse is defined by density changes. Moreover, from the perspective of four-dimensional space, the two real dimensions of time are observed along a single imaginary axis. (3.7)

$$e = \sqrt{1 - \frac{x^2}{y^2}} \quad \epsilon = \sqrt{1 + \frac{x^2}{y^2}}$$

$$f\left(\rho(k,l,m)\right) \propto e \quad \sec\left(sin^{-1}\left(\log_{x_k}\left(\frac{x_l}{x_m}\right)\right)\right) = \frac{1}{\sqrt{1 - \frac{\left(\ln\left(\frac{x_l}{x_m}\right)\right)^2}{\left(\ln\left((x_k)\right)\right)^2}}} \qquad 3.7$$

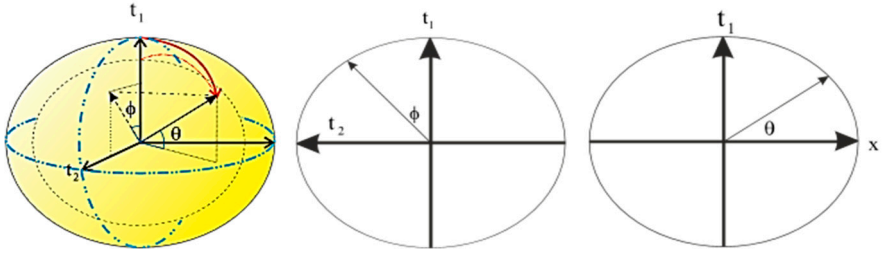


**Figure 6.** Variations in density lead to the eccentricity of the ellipse, and this eccentricity, in turn, generates an inner centrality within the closed manifold. Consequently, the rigid body co-rotates with the expansion of space around the mass field.

The fundamental principle of selections in the dimensions of time is rotation. A simple example of this type of rotation is based on the Möbius manifold. Due to the imaginary nature of time dimensions from the observers' perspective, the phase shift of the seesaw function is accompanied

 doi:10.20944/preprints202505.1200.v1



by rotation within Möbius space. The Constriction Point and Expansion Region in Möbius space are the main factors in the entanglement phenomenon. The geometric Bernoulli principle connects geometric action along the manifold with the wave function. A simple example of this phenomenon is the deformation of shapes on a closed spherical surface during deviation from sphericity. The equivalence of the laws of wormholes and entanglement depends on the geometric Bernoulli principle within Möbius space. The concept of tides on a rotating spherical surface and the increasing speed of ships on the water's surface is a simple instance of manifold information. (3.8)

$$\left(\frac{\left(\frac{tan^{-1}(\varphi)-\left(\frac{180}{\pi}\right)}{2\pi}\right)^3\left(\frac{1}{6}\right)\pi^3}{c}\right)=G$$

$$P+\frac{1}{2}\rho v^2+\rho gh \Longrightarrow \left(\frac{1}{2}\right)^6\pi^3\rho c^2+\rho\sqrt{1-(\partial\rho)^2}\left(\frac{\left(\frac{tan^{-1}(\varphi)-\left(\frac{180}{\pi}\right)}{2\pi}\right)^3\left(\frac{1}{6}\right)\pi^3}{c}\right) \qquad 3.8$$

$$\Psi(t_1,t_2,\phi)=\Psi_0.e^{i\theta(\phi)}.sin(\frac{2\pi\omega t_1,t_2}{T})$$

θ(ϕ) is the phase shift resulting from rotation in Möbius space.

The connection between the phenomenon of entanglement and prime numbers depends on the proof of the Riemann Hypothesis. The critical strip of the Riemann zeta function for prime numbers at the point 0.5 forms a golden spiral perpendicular to the plane.

(**Figure 7**) The outcome of the zeta function for primes can be represented as an eccentric ellipse oriented at an angle in complex space with two imaginary axes. Prime number groups are distributed along specific angles from the spiral's center. According to the Goldbach conjecture, and considering the preservation of parity in multiplication (except for the number 2), the role of prime numbers in predicting the effect of observation over time becomes significant. (3.9)

$$\zeta\zeta^*=sin^2(\theta)\longrightarrow P_\mu+P_\upsilon\longrightarrow 90\pm i\phi_{G_{\mu+\upsilon}}\quad P.n_\alpha=\alpha\ldots\qquad P.n_\beta=\beta\ldots\quad P\neq 2$$

$$\theta_{G_1}A\quad\theta_{G_2}B\quad\rightarrow\quad 2\sin\left(\frac{\phi}{2}\right)e^{-cos^2(\theta)} \qquad 3.9$$

The Fibonacci logarithmic spiral, defined by a logarithmic secant function with base 2 and driven by the INDS (Inner Digit Sum) of prime numbers, generates phase differences that converge with the eccentricity of ellipses. Here, r is the radial distance from the spiral center, θ is the angle in radians, a is a subset of prime numbers, and b is the spiral's growth rate, equal to the golden ratio. (3.10)

$$r=ae^{b\theta}\quad b=\frac{1}{\tan\left(\frac{1+\sqrt{5}}{2}\right)}\quad,\quad a\in P$$

$$sec^{-1}(2)=cos^{-1}\left(\frac{1}{2}\right)\implies P_n=\alpha\beta\ldots\eta\rightarrow sec^{-1}\left(2^\alpha 2^\beta\times\ldots\times 2^\eta\right) \qquad 3.10$$

Accordingly, if the spiral is perpendicular to the critical strip of the zeta function, then sin θ, representing the eccentricity of the ellipse, is directly related to the distribution of prime numbers. (3.11)

$$\sin\left(cos^{-1}\left(\frac{1}{n}\right)\right)=\sqrt{1-\frac{1^2}{n^2}}=1/sec(sin^{-1}(\log_n(\frac{\partial\rho}{\partial x})) \qquad 3.11$$

$$\ln\left(\frac{1+\sqrt{5}}{2}\right)\approx\left(\frac{1}{2}\right)^6\pi^3$$

Preprints.org (www.preprints.org) | NOT PEER-REVIEWED | Posted: 15 May 2025 doi:10.20944/preprints202505.1200.v1



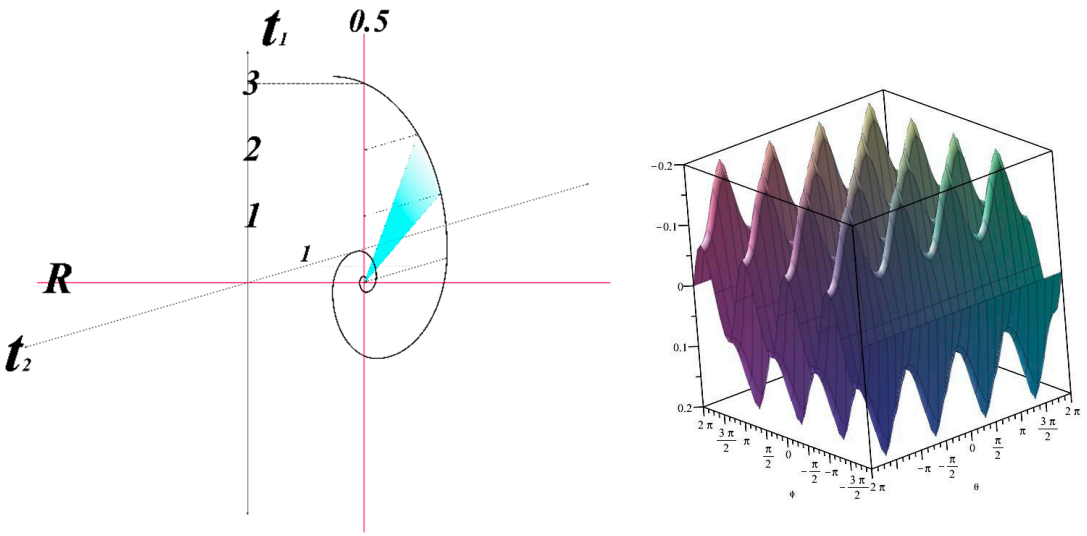


**Figure 7.** The invariance of the angular properties of the spiral demonstrates the connection among prime numbers across different groups. Furthermore, the ratio between temporal and spatial dimensional stresses gives rise to both the golden ratio and the golden spiral. The 0.5 strip in the zeta function highlights the differentiability of the Taylor expansion at the critical point 0.5, linking the golden ratio to hypergeometric distributions within wave function packets.

Trigonometric ratios are derived from the curvature of the golden spiral in complex space and are formulated based on the distribution of prime numbers. The vertical spiral within the critical strip of the Riemann zeta function forms two polar angles with respect to the coordinate origin. Accordingly, two right-angled triangles sharing a common side from the origin exhibit trigonometric ratios directly related to prime numbers. Based on this geometric framework, Möbius space is associated with the characteristic angles of 45°, 30°, and 60°. (3.11) Figure 8

$$\left(\frac{2\sin(60)+1}{2\cos(60)+2i}\right)\left(\frac{2\sin(60)-1}{2\cos(60)-2i}\right)=\left(\frac{1-\sqrt{3}}{2i-1}\right)\left(\frac{1+\sqrt{3}}{2i+1}\right)=2/5$$

$$\left(\frac{2\sin(30)+1}{2\cos(60)+2i}\right)\left(\frac{2\sin(30)-1}{2\cos(60)-2i}\right)=\left(\frac{0}{2i-1}\right)\left(\frac{2}{2i+1}\right)=0$$

$$\left(\frac{2\sin(45)+1}{2\cos(60)+2i}\right)\left(\frac{2\sin(45)-1}{2\cos(60)-2i}\right)=\left(\frac{1-\sqrt{2}}{2i-1}\right)\left(\frac{1+\sqrt{2}}{2i+1}\right)=1/5$$

$$\left(\frac{2\sin(30)+1}{2\cos(45)+2i}\right)\left(\frac{2\sin(30)-1}{2\cos(45)-2i}\right)=\left(\frac{0}{2i-\sqrt{2}}\right)\left(\frac{2}{2i+\sqrt{2}}\right)=0$$

$$\left(\frac{2\sin(45)+1}{2\cos(45)+2i}\right)\left(\frac{2\sin(45)-1}{2\cos(45)-2i}\right)=\left(\frac{1-\sqrt{2}}{2i-\sqrt{2}}\right)\left(\frac{1+\sqrt{2}}{2i+\sqrt{2}}\right)=1/6 \qquad 3.11$$

$$\left(\frac{2\sin(30)+1}{2\cos(30)+2i}\right)\left(\frac{2\sin(30)-1}{2\cos(30)-2i}\right)=0 \qquad M\{1,-1,-1,0,-1,1\}$$

 doi:10.20944/preprints202505.1200.v1



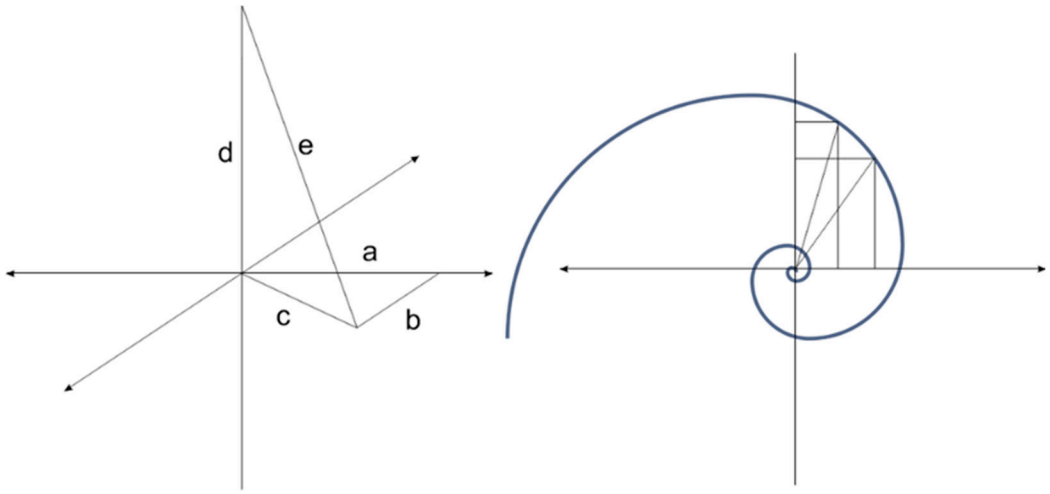


**Figure 8.** Two right-angled triangles with a shared side, embedded in complex space, establish a connection between the Fibonacci spiral and the critical strip of the Riemann zeta function through trigonometric ratios derived from prime numbers. The logarithmic Fibonacci spiral is orthogonal to the critical strip, reflecting the angular distribution of prime-number structures in the complex plane.

## 4. CHSH and INDS

The Fibonacci logarithmic spiral converges with a logarithmic secant function. The secant function is based on 2 and the explanation of the INDS of prime numbers. The eccentricity of the ellipse is the factor of convergence between the golden spiral and the secant function. The eccentricity of the ellipse is also the factor of overlap between prime numbers and the secant function. Therefore, the spiral metric of Möbius space, which depends on density, is obtained. The metric possesses five symmetric and mirror-like degrees that examine the behavior of functions over time (before, after). (4.1)

$$g_{\mu\nu} = \begin{bmatrix} ra^2cos^2\theta\ cos^2\phi & 0 & 0 & 0 & 0 & 0 \\ 0 & r^2a^2cos^2\theta & 0 & 0 & 0 & 0 \\ 0 & 0 & r^2a^2 & 0 & 0 & 0 \\ 0 & 0 & 0 & a^2r^2 & 0 & 0 \\ 0 & 0 & 0 & 0 & a^2r^2sin^2\theta & 0 \\ 0 & 0 & 0 & 0 & 0 & a\ r^2sin^2\theta\ sin^2\phi \end{bmatrix}$$

$$M\{1,-1,-1,0,-1,1\}$$

$$\boldsymbol{cos^2\left(cos^{-1}\left(\frac{p_n}{p_{n+1}}\right)\right) = P_{diff}} \qquad 4.2$$

Based on a statistical sample from the CHSH experiment (See **Table 4**), and the existence of a mean constant value for entangled particles, along with a correlation function for similar outcomes, the role of prime numbers in the structure of space-time, wormholes, and entanglement emerges considering the number of sines and cosines in the six-dimensional metric. This metric links the hidden variable a,r through the phenomenon of entanglement to the structure of space. Based on the comparison of the empirical observation chart from the CHSH experiment and the group intervals, the role of observation in the continuity of entangled structure within space-time becomes apparent. **Figures 9–11**

$$-a^2r = -\quad -a^2r^2 = -\quad -r^2a^2 = -\quad a^2r^2 = ++\quad a^2r^2 = ++\quad a\ r^2 = ++$$

$$9 \longrightarrow ++ \qquad 3 \longrightarrow - \qquad 4.3$$

 doi:10.20944/preprints202505.1200.v1



**Table 4.** Placement of the numbers 3, 6, and 9 in the CHSH experiment.

| By | Bx | Az | Ay | Ax |
|---|---|---|---|---|
| 3 | 3 | 9 | 9 | 9 |
| 3 | 3 | 3 | 9 | 9 |
| 9 | 3 | 9 | 3 | 9 |
| 9 | 3 | 3 | 3 | 9 |
| 3 | 9 | 9 | 9 | 3 |
| 3 | 9 | 3 | 9 | 3 |
| 9 | 9 | 9 | 3 | 3 |
| 9 | 9 | 3 | 3 | 3 |

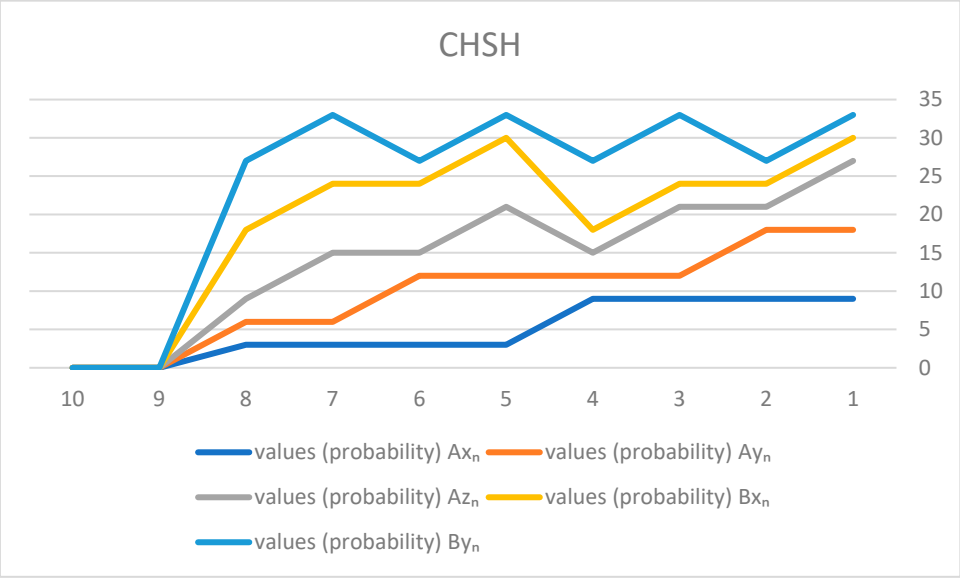


**Figure 9.** Observation, based on the space-time structure associated with prime number groups, identifies states that preexist within the fabric of space-time. Additionally, the collapse and state transitions of the wave function influence the future states of the second entangled particle.

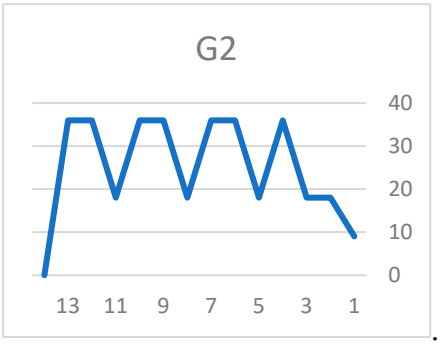


**Figure 10.** The similarity between the targeted CHSH experiment and Group 2 oscillations reveals hidden correlations within the space-time structure.

 doi:10.20944/preprints202505.1200.v1



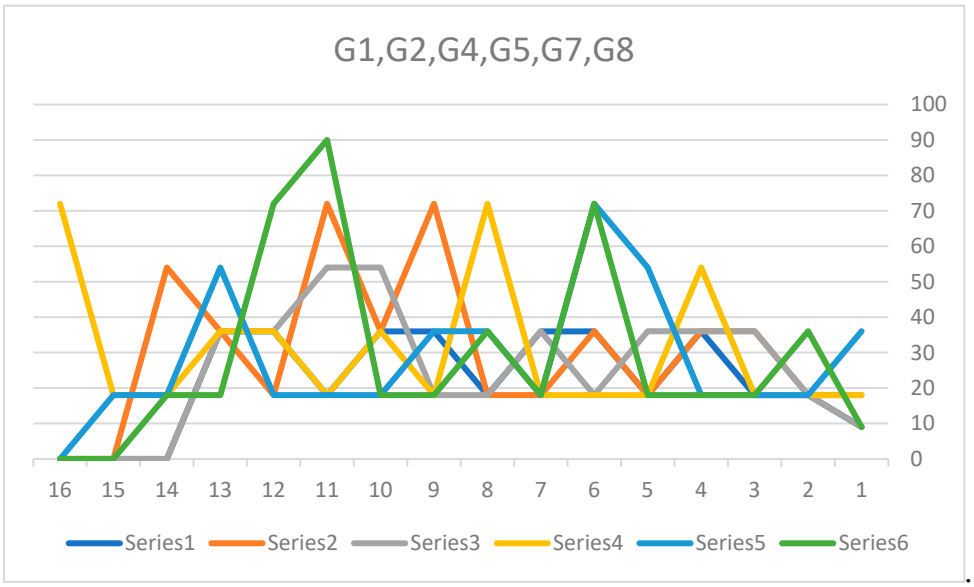


**Figure 11.** The correlation of the columns 3, 6, and 9 in the classification of prime numbers with the phenomenon of entanglement in three dimensions is clearly evident. The squared sine and cosine functions of the metric define geometric oscillations and turbulence of space-time due to density fluctuations. Columns 3, 6, and 9 enable the modulation of density fluctuations within six-dimensional space, linking them to space-time geodesics.

## 5. Geometric Origin of Temporal Correlation from Density Symmetry in Expanding Möbius Space

Based on the three-dimensional structure of matter, the geometric stresses exerted by the expanding Möbius space cause the motion and rotation of density around the mass field. This rotation is isotropic and aligned with the movement of the field in the real-time dimension and the arrow of time. Therefore, the Coriolis effect in the present moment between objects with identical density induces a reverse effect similar to entangled states. Rotational symmetry of the geometric Coriolis effect depends on density and the diversity of wave function packets. Observation in the fluctuating and turbulent quantum space causes density variations in particles of identical density, and the tidal effect in time is entirely dependent on the orientation of the observation. **Figure 12** This means that no force akin to tidal interactions is exchanged between two entangled particles; rather, the observer measures states arising from the oscillation of the space-time structure. A simple example of this effect is the state of leaves on the surface of a pond in turbulence. Two particles on the surface of an expanding sphere are located in the negative z-dimension relative to one another. As the shell rotates over time, they enter each other's spatial states. This effect generates correlation across time. **Figure 13**

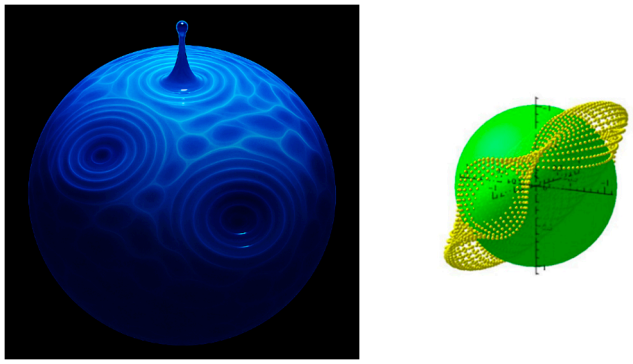

 doi:10.20944/preprints202505.1200.v1



**Figure 12.** Two entangled particles are geometrically connected only through the time dimension in space, like two opposite points on the surface of a sphere. The geometric Coriolis effect, through a seesaw function, generates a tidal geometric effect across two-time dimensions. Given the expansion of the sphere in image and the arrow of time, the particles are situated in each other's past dimension. And due to the rotational effect of the expanding sphere, the displacement of spatial states in the time dimension produces continuity and the violation of Bell's inequality.

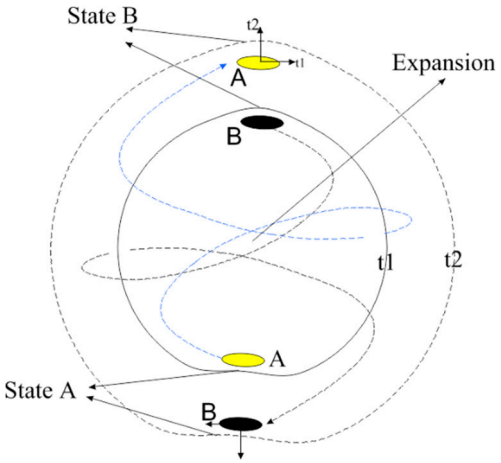


**Figure 13.** Two one-dimensional objects are positioned on the surface of an expanding three-dimensional sphere, moving in opposite directions. From their perspective, the Z and Y dimensions are imaginary. Additionally, both objects perceive these two dimensions along a single unified axis. Point B, from the viewpoint of point A, is located in the past, and similarly, point A appears in the past from point B's perspective. As the sphere expands, the state of both points shifts along a helical trajectory. Density fluctuations on the sphere's surface are uniformly distributed. Consequently, the choices of Alice and Bob reflect the natural correlation of events over time.

The geometric Coriolis tensor in expanding Möbius space accounts for the generation of fundamental forces through geometry. These forces, shaped within the natural Constriction Points and spatial gaps of the Möbius manifold, follow a geometric version of Bernoulli's principle. The natural gaps in each modulus of prime number groups represent recurrent phases of these spatial ruptures. Irregularities within each group arise from fluctuations driven by expansion and the underlying space-time geometry. These groups are positioned on a hyper spherical structure with a five-dimensional metric and a total surface area of $\pi^3$. When this hypersphere is projected onto a two-dimensional plane, both order and apparent randomness become observable. The gaps between prime clusters correspond to discontinuities in the shell of the five-dimensional sphere.

These gaps are wormholes within the structure of spacetime. The stress of the geometric Coriolis tensor of momentum and energy generates another inverse tensor that ensures rotation within phase space. The K-tensor is the reflection of the momentum stress tensor in the future and functions like a butterfly effect: without violating causality, it transforms the effect into the origin of the cause. Based on this, dark matter and dark energy are the butterfly effect echoes of mass and energy across time, within the closed manifold of Möbius space. This phenomenon is also antisymmetric in the temporal dimensions, similar to the Coriolis effect (the six-dimensional energy-momentum tensor). (5.1)

$$\left|K_{\mu\nu}\right| = \left(\frac{{r_t}^3}{\pi c^3 {r_x}^3}\right) h^2 G^2 e^{(\varphi)^2\pi^3} = \left(\frac{{r_t}^3}{\pi c^3 {r_x}^3}\right) 3.5104354766 \times 10^{-52} = \Lambda$$

$$T^{\mu\nu} = \begin{bmatrix} 0 & 0 & 0 & 0 & 0 & -\rho^{\dagger} \\ 0 & 0 & 0 & 0 & -\rho & 0 \\ 0 & 0 & 0 & \rho & 0 & 0 \\ 0 & 0 & P & 0 & 0 & 0 \\ 0 & P & 0 & 0 & 0 & 0 \\ P & 0 & 0 & 0 & 0 & 0 \end{bmatrix} \qquad T_{\mu\nu} = \begin{bmatrix} -\rho^{\dagger} & 0 & 0 & 0 & 0 & 0 \\ 0 & -\rho & 0 & 0 & 0 & 0 \\ 0 & 0 & \rho & 0 & 0 & 0 \\ 0 & 0 & 0 & P & 0 & 0 \\ 0 & 0 & 0 & 0 & P & 0 \\ 0 & 0 & 0 & 0 & 0 & P \end{bmatrix}$$

 doi:10.20944/preprints202505.1200.v1



$$K_{\mu\nu} = \begin{bmatrix} \frac{r_t}{\pi c} & 0 & 0 & 0 & 0 & 0 \\ 0 & \frac{r_t h e^{\pi^3}}{c} & 0 & 0 & 0 & 0 \\ 0 & 0 & \frac{r_t\sqrt{G} h e^{\varphi^2}}{c} & 0 & 0 & 0 \\ 0 & 0 & 0 & \frac{\sqrt{G}}{r_x} & 0 & 0 \\ 0 & 0 & 0 & 0 & \frac{\sqrt{G}}{r_x} & 0 \\ 0 & 0 & 0 & 0 & 0 & \frac{\sqrt{G}}{r_x} \end{bmatrix} \quad 5.1$$

The preservation of causality within the one-way nature of the butterfly effect arises from the contravariant influence of the future on the past, acting as an echo of the momentum-energy tensor. This effect can alter the oscillatory geodesic states hidden in the past. For example, modifying the polarization of light through hidden correlations over time becomes possible. (5.2)

$$\acute{P}(t) = P_0 . e^{-i\gamma t_-} e^{-i\omega t_+} e^{-i\delta t} sin^2(\theta) sin^2(\phi) \quad 5.2$$

The curvature of space-time caused by mass and energy, over time, defines the wave-like behavior of matter. The Einstein field tensor for extremely small masses has non-zero components only in the temporal dimension. Consequently, the higher-dimensional wave function tensor unveils the geometric-spin Coriolis effect embedded within space-time. (5.3)

$$G_{\mu\nu} = \begin{bmatrix} \frac{10}{r^2} & 0 & 0 & 0 & 0 & 0 \\ 0 & \frac{4}{r\ cos^2\phi} & 0 & 0 & 0 & 0 \\ 0 & 0 & \frac{4}{r\ cos^2\theta cos^2\phi} & 0 & 0 & 0 \\ 0 & 0 & 0 & \frac{4}{r\ cos^2\theta cos^2\phi} & 0 & 0 \\ 0 & 0 & 0 & 0 & \frac{4\ sin^2\theta}{r\ cos^2\theta cos^2\phi} & 0 \\ 0 & 0 & 0 & 0 & 0 & \frac{4\ sin^2\theta\ \ sin^2\phi}{r\ a\ cos^2\theta cos^2\phi} \end{bmatrix}$$

$$\Psi_{\mu\nu} = \begin{bmatrix} cos^2\theta\ cos^2\phi & A_\iota & A_\iota & A_\iota & A_\iota & A_\iota \\ A_\iota & cos^2\phi & A_\iota & A_\iota & A_\iota & A_\iota \\ A_\iota & A_\iota & e^{-i\pi\varphi} & A_\iota & A_\iota & A_\iota \\ A_\iota & A_\iota & A_\iota & e^{i\pi\varphi} & A_\iota & A_\iota \\ A_\iota & A_\iota & A_\iota & A_\iota & sin^2\theta & A_\iota \\ A_\iota & A_\iota & A_\iota & A_\iota & A_\iota & sin^2\theta\ sin^2\phi \end{bmatrix} \quad 5.3$$

$$A_\iota = \pm\left(\frac{\pi}{3}\right), \pm\left(\frac{2\pi}{3}\right), \pm(\pi)\ , \pm\left(\frac{4\pi}{3}\right)\ , \pm\left(\frac{5\pi}{3}\right)\ ,\ \pm(2\pi),\ \iota = 1,2,3,4,5,6$$

Free fall in a gravitational field depends on two dimensions of time, leading to a general equation that applies to both the microscopic and macroscopic worlds. (5.4)

$\mu, \nu = 1,2,3,4,5,6$

$$\Psi_{\mu\nu} + R_{\mu\nu} - \frac{1}{2} R g_{\mu\nu} + \Lambda g_{\mu\nu} = \left(\frac{\pi-2}{2}\right)^6 \left(\frac{he}{c}\right) T_{\mu\nu} + K_{\mu\nu} \quad 5.4$$

Small wavefunction packets are directly proportional to the wavelength. Accordingly, density variations determine the packet length in real space. Given the Möbius rotation of space over time, the phase shift of electromagnetic waves and wavefunction packets is governed by density fluctuations across two temporal dimensions. As a result, discrete blackbody radiation and the temperature density relationship are defined. Based on the tension applied over time in the expanding Möbius space and the rotation of the Möbius space, the wavelength is defined oscillatory

Preprints.org (www.preprints.org) | NOT PEER-REVIEWED | Posted: 15 May 2025 doi:10.20944/preprints202505.1200.v1



as dependent on the hypergeometric distribution of wave packet functions. This phenomenon describes the wave-particle duality. (5.5) **Figure 14**

$$\frac{\lambda\,(t)}{c} \sim \frac{1}{cos^2\theta\ cos^2\phi}.\frac{1}{\omega}\ \sim L_{\tilde{\psi}}\ ,\frac{h}{mv} = \lambda$$

$$\Rightarrow \left|\tilde{\psi}_1\right\rangle = \frac{h}{r\ cos^2\theta\ cos^2\phi} \qquad \chi = sin^2\theta\ sin^2\phi sin^2\theta$$

$$|\Psi\rangle = \frac{h\upsilon(e^{-ikr^2\chi})}{a^4r^3cos^2\theta\ cos^2\phi\ cos^2\phi\ \pi} \qquad T_{(\rho)} \equiv \frac{\hbar c}{k_b}.\left(\frac{\partial^2\sqrt{1+(\partial\rho)^2}}{\partial(sec(sin^{-1}(log_n(\frac{\partial\rho}{\partial x})))^2}\right)^{\frac{1}{4}} \qquad 5.5$$

$$\lambda \approx \frac{h}{(m\rho c)^{\frac{1}{2}}}.e^{i\pi\varphi}$$

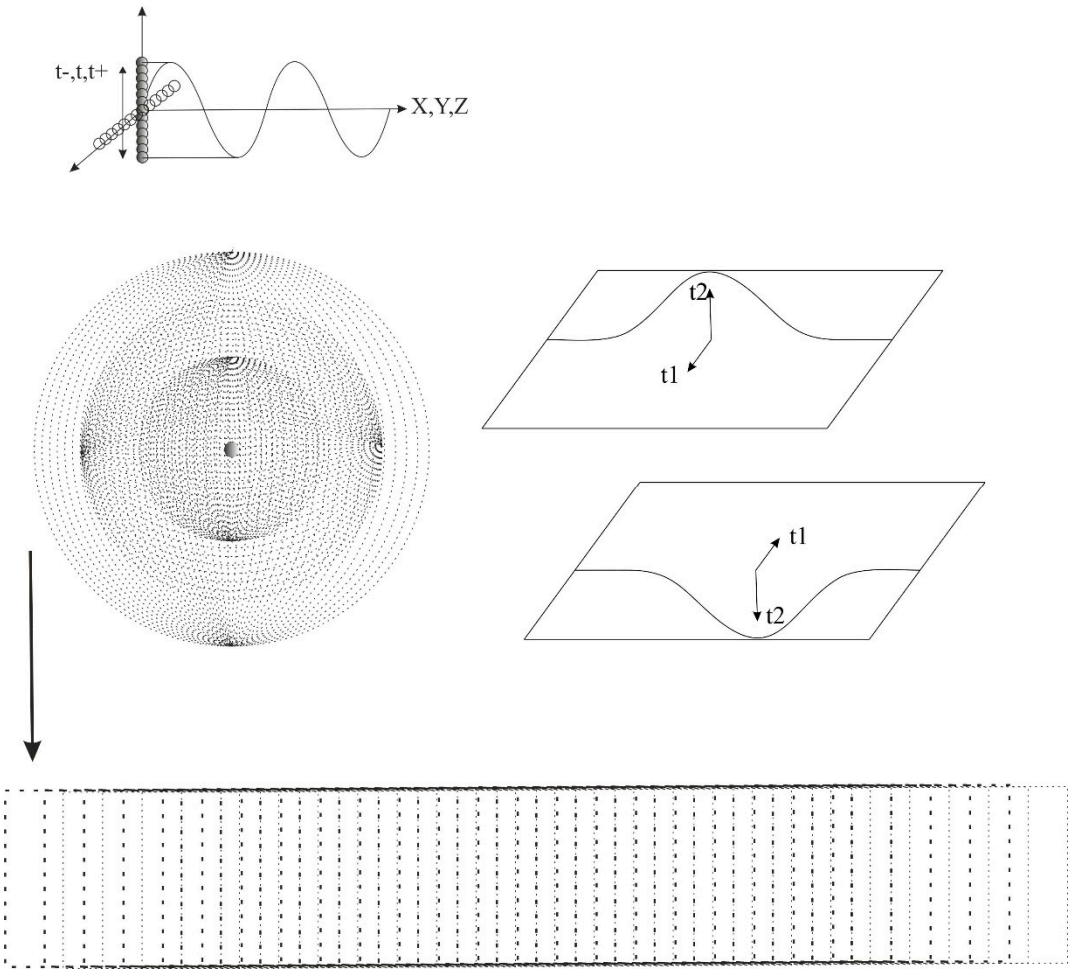


**Figure 14.** The oscillation in two orthogonal dimensions of time demonstrates the quantization of electromagnetic waves. It also establishes a direct connection between the changing particle states and the rotating Möbius space, thereby linking the wave-particle phenomenon.

## 6. Result and Discussion

As a result of this research, the convergence between the prime number function and the correlation function of the woven space-time structure described by the spiral embedded within the critical strip of the Riemann zeta function makes it possible to identify the causes and influencing factors of the entanglement phenomenon while preserving the laws of special relativity and quantum mechanics. The mechanism that prevents causality violation within the unidirectional butterfly effect

 doi:10.20944/preprints202505.1200.v1



is the contravariant reflection of the momentum-energy tensor. This ensures that the influence of the future on the past does not invert the origin, but instead causes space itself to expand, generating what we perceive as dark energy. The preservation of causality within this one-way butterfly effect stems from the contravariant configuration of the momentum-energy tensor (i.e., a reversed time-arrow), in which the influence of the future on the past is attenuated through reversed resonance via a wormhole. However, informational intuitions affect the past through wormholes sustained by entangled correlations embedded in the fabric of space-time. Causality operates solely by transmitting compact information pulses from higher-dimensional Hilbert space (time-dependent) to lower dimensional reality much like a prism governed by density gradients, or a sender from higher dimensions inscribing messages on the surface of an expanding sphere. The only viable method for this transmission is the compression and decoding of intuitive signals. Time is not a singular linear entity, but a three-dimensional construct, comprising the past ($t_1$), present ($t_2$), and future ($t_3$). Information inherently belongs to time, defined by sequence and causality, whereas matter and energy are essential constituents of space, characterized by position and extension. Therefore, it follows that spacetime is fundamentally six-dimensional, encompassing three spatial and three temporal dimensions. (6.1)

$$\partial(\rho) = \partial t \qquad 6.1$$

A two-dimensional surface on an expanding sphere can be compared to a Möbius space, provided there is rotation during expansion. Accordingly, from the perspective of a one-dimensional space on the sphere's surface, the y and z dimensions are observed along an imaginary axis. Based on this, time has both orthogonal and intrinsic dimensions. **Figure15**

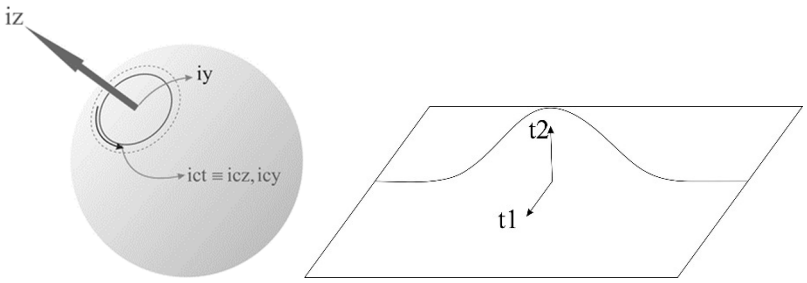


**Figure 15.** The z and y dimensions on the surface of the expanding sphere are imaginary from the perspective of a one-dimensional space and are viewed along a single axis.

We therefore define the spherical metric as a function of the ellipse's eccentricity based on heterogeneity arising from variations in density within the geometric structure of space-time. Intrinsic expansion arises from the absence of matter and energy in other dimensions, and the passage of time is the motion of objects in the true dimension of time. Accordingly, the energy-momentum tensor and the force tensor, which are responsible for creating spin, establish the relationship between density and time. Density is like a length in spacetime rotating around a mass field. The rotation caused by geometric stress creates fundamental constants of physics. (6.2)

$$\left(\frac{\left(\frac{1}{2\pi}\right)^3+\left(\frac{1}{2}\right)^6\pi^3\left(\frac{1}{6}\right)\pi^3\left(\frac{\left(\frac{3\pi-6}{2\pi}\right)}{360}\right)\varphi^3}{c}\right) \cong 6.6765834\times10^{-11} \cong G \qquad 6.2$$

$$\left(\frac{\left(\frac{1}{2\pi}\right)^3+\left(\frac{1}{2}\right)^6\pi^3 e^{\tan\left(\frac{180}{\pi}\right)}}{c^2}\right)^2 = 6.5693903027\times10^{-34} \cong h$$

$$h^2G^2e^{(\varphi)^2\pi^3} = \Lambda$$

 doi:10.20944/preprints202505.1200.v1



Matter and energy are embedded in the real dimension of the present time. Two entangled particles, regardless of large spatial separation, remain correlated through the latent oscillatory structure of space, due to shared density states. The symmetry arising from the self-expansion of space induces degrees of freedom for matter and energy in lower dimensions. When Alice measures her particle, she observes the future state of Bob's particle, and Bob observes the future state of Alice's. In the subsequent measurement, Alice detects Bob's past state, and vice versa. The next measurement occurs in a fuzzy space and may repeat previous states depending on conditions .Temporal correlation is demonstrated through the space-time structure governed by six groups of prime numbers, treated as a continuous and oscillatory medium. Accordingly, experimental apparatuses can be configured to classically demonstrate entanglement. The fundamental condition for correlation between two events is the spatial shift of the observer and the measuring component . Even if instantaneous influence occurs on an information set, due to displacement of experimental elements, special relativity remains unviolated under proper temporal coordinates .This indicates that density variation influences entanglement: for instance, a particle within a gravitational field cannot remain entangled with a particle outside the field. **Image 1**

**Image 1:** The image of surface turbulence in the Y and Z dimensions within a two-dimensional manifold reveals a direct correlation between density changes, radiation, oscillation, and inherent time-dependent correlations.

According to the INDS sum, symmetric and mirror primes exhibit identical properties. Therefore, one can analyze the gaps and discontinuities within Möbius space. The fountain-like and hopping behavior between prime groups is directly linked to mirror numbers. **Image 2**. The water droplets emerging from the spinning fountain simultaneously hit the surface of the water. The produced spectrum can be decomposed into various frequencies using FFT. An important issue is the correlation between the distances of impact points and different sound frequencies. This phenomenon bears strong similarity to the radiation, color, and temperature of a black body, which can only be analyzed through the six groups (INDS) of prime numbers. The human brain predicts the subsequent wave function states in time by comparing the inverse of current information with memory, based on the existence of correlation in the space-time structure.[8]

 doi:10.20944/preprints202505.1200.v1



**Image 2:** Based on the gaps formed between the groups (Table 1) and the observation of symmetric and mirror reflected numbers, the resulting fields from these discontinuities appear as numerically symmetric and reflective across the groups**.**

This effect, analogous to the distortion caused by projecting a spherical surface onto a plane, is transferred to the prime number groups through the inhomogeneous structure of surface area and hyperspheres. To experimentally test dimensions and prime groups, two types of clocks can be constructed one based on 60 seconds and the other on 100 seconds, each assigned to two orthogonal time dimensions. For example, to convert standard hours and minutes to a 100-minute clock, we use relation (6.3).

$$(h_{60} \times 60) + \big((h_{60} - 1) \times 40\big) = h_{100} \qquad 21{:}42 \rightarrow (21 \times 60) + (20 \times 40) + 42 = 21{:}02 \qquad 6.3$$

Using the subtraction of INDS sums, one can trace oscillatory spatial variations tied to prime numbers in six distinct groups. Additionally, the possibility of adjusting and observing correlations related to columns 3, 6, and 9 has been studied and tested by transforming paired and mirror hours. Entanglement control for compressed information transfer based on the brain's reward and error system has been examined. [9] Let Δn denote the absolute difference between a number and its digit-reversed form. (6.4)

$$digit\ reversal\ of\ n = rev(n) \Rightarrow rev(2079) = 9702$$

$$\Delta n = |n - rev(n)| \Longrightarrow 9702 - 2079 = 7623 \Rightarrow 7623 - INDS\big(INDS(7623)\big) = 7614$$

$$INDS(21) = INDS(12) \qquad 21{:}21 \rightarrow 2081 - INDS\big(INDS(2081)\big) = 2079$$

$$\frac{2079}{9} = 231$$

$$h_{100}(21{:}12) = 2072$$

$$\Longrightarrow 21{:}12 \rightarrow \overrightarrow{M9} = 230 \quad 21 - 12 = 9 \qquad 6.4$$

$$rev(2072) - 2072 = 630$$

$$(14{:}14{,}14{:}41) = 155 - 152 = 3 \qquad 41 - 14 = 27$$

Accordingly, the persistence of identical observational outcomes within a defined correlation becomes predictable through the temporal evolution of the wave function. (6.5)

$$\theta_{14} = \frac{14}{60} \times 360 = 84^{\circ} \quad \theta_{12} = 72^{\circ} \quad 84^{\circ} - 72^{\circ} = 12^{\circ} \quad Min\ _{\theta} = \frac{12^{\circ}}{360} \times 60 = 2^{''} \qquad 6.5$$

The difference between the first and second phases of INDS modulo 9 is always 1 (6.6)

 doi:10.20944/preprints202505.1200.v1



$$\frac{7614}{9} = 846 \qquad 7623 - INDS(7623) = 7605 \longrightarrow \frac{7605}{9} = 845 \qquad 6.6$$

We examine the geometric potential difference, derived from the INDS analogy, in two distinct configurations for the CHSH experiment. The result expresses the temporal coordinates of the Möbius space manifold. (6.7)

$$sec\left(sin^{-1}\left(\left|\left(\log_2\left(\frac{\Delta n(h_{60})}{360}\right)\right)\left(log_2\left(\frac{\Delta n(h_{100})}{360}\right)\right)\right|\right) = \frac{1}{\sqrt{1+\frac{\left(\ln\left(\frac{\Delta n(h_{60})}{360}\right)\right)^2\left(ln\left(\frac{\Delta n(h_{60})}{360}\right)\right)^2}{(ln(2))}}} = R$$

$$\theta, \phi \, \epsilon \, tan^{-1}\left(R\sqrt{1-\frac{\left(ln\left(\frac{\Delta n(h_{60})}{360}\right)\right)^2\left(ln\left(\frac{\Delta n(h_{60})}{360}\right)\right)^2}{(ln(2))}}\right) \qquad 6.7$$

Through compression and temporal decoding, it becomes feasible to transmit and receive information faster than light. (6.8) The possibility of information transfer in entangled pairs through the metric structure is feasible. **Figure16**

$$|(\langle 0|\otimes\langle a_0|)|\varphi\rangle|^2 = \frac{1}{2}cos^2\frac{\pi}{8} \quad ,|(\langle 1|\otimes\langle a_1|)|\acute{\varphi}\rangle|^2 = \frac{1}{2}cos^2\frac{\pi}{8}$$

$$|\varphi\rangle = \frac{1}{\sqrt{2}}(|00\rangle + |11\rangle) \qquad |(|1\rangle\otimes|a_1\rangle)\langle\acute{\varphi}||^2 = E \qquad |(\langle 1|\otimes\langle b_1|)|\acute{\varphi}\rangle|^2 = K$$

$$g_{\mu\nu} = \begin{bmatrix} ra^2|(\langle 0|\otimes\langle a_0|)|\varphi\rangle|^2K & 0 & 0 & 0 & 0 & 0 \\ 0 & r^2a^2|(\langle 1|\otimes\langle a_1|)|\acute{\varphi}\rangle|^2 & 0 & 0 & 0 & 0 \\ 0 & 0 & r^2a^2\langle\acute{\varphi}|\varphi\rangle & 0 & 0 & 0 \\ 0 & 0 & 0 & a^2r^2\langle\varphi|\acute{\varphi}\rangle & 0 & 0 \\ 0 & 0 & 0 & 0 & a^2r^2|(|1\rangle\otimes|b_1\rangle)\langle\varphi||^2 & 0 \\ 0 & 0 & 0 & 0 & 0 & a\ r^2|(|0\rangle\otimes|b_0\rangle)\langle\varphi||^2E \end{bmatrix} \qquad 6.8$$

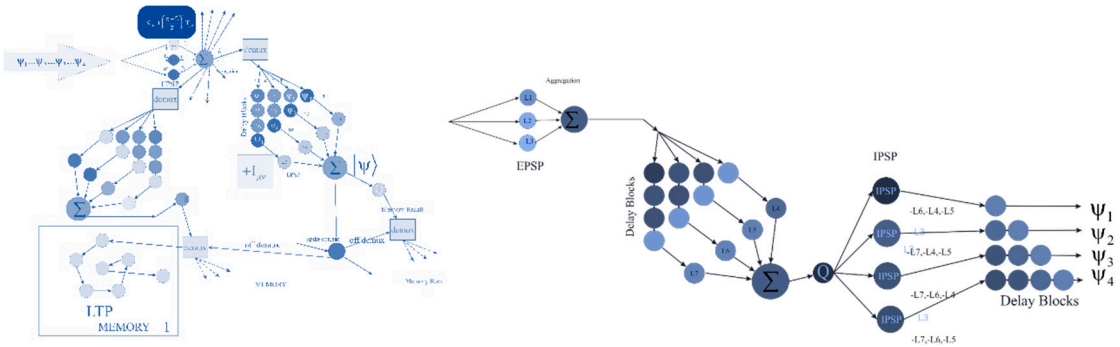


**Figure 16.** Information is encoded over time based on the INDS classification of prime numbers into columns 3, 6, and 9. After temporal accumulation, the data is grouped and compressed into defined time units. The EPSP excitation coefficients are encoded using the intervals within one of the prime number groups, along with the compressed data, and are stored in memory. At regular time intervals, both systems can, through information reversal and network decoding, receive new data from the temporal structure via entanglement.

**Statement 1:**

*All material outcomes derived from this theoretical work, including future inventions, remain the intellectual property of Seyed Kazem Mousavi(https://orcid.org/0000-0002-2961-284X) and Elham Razzazi. (8)*

## References

1. Cowen, Ron. "Space, time, entanglement." *Nature* 527.7578 (2015): 290.https://doi.org/10.1038/527290a
2. Bhushan, Sanjay. "The Cosmic Dynamics of Constructive Resonance, Energy Transformation and Alternating States of Universe: A Modified Systemic Perspective of Einstein Field Equations (EFE)." *Energy*

 doi:10.20944/preprints202505.1200.v1



*Transformation and Alternating States of Universe: A Modified Systemic Perspective of Einstein Field Equations (EFE)(January 31, 2025)* (2025).

3. Simon, David S. "EPR, Bell Inequalities, and Local Realism." *Introduction to Quantum Science and Technology*. Cham: Springer Nature Switzerland, 2025. 417-429.https://doi.org/10.1142/S2424942424500063
4. Barbarani, Vito. "A Quantum Model of the Distribution of Prime Numbers and the RIEMANN hypothesis." *International Journal of Theoretical Physics* 59.8 (2020): 2425-2470.https://doi.org/10.1007/s10773-020-04512-2
5. Alminawi, Mohammad, Ilaria Brivio, and Joe Davighi. "Jet bundle geometry of scalar field theories." *Journal of Physics A: Mathematical and Theoretical* 57.43 (2024): 435401.https://doi.org/10.4099/math1924.13.235
6. Zhang, Lei, et al. "Co-Prime Modulation for Space-Time-Coding Digital Metasurfaces with Ultralow-Scattering Characteristics." *Advanced Functional Materials* 34.21 (2024): 2314110. https://doi.org/10.1002/adfm.202314110
7. Mousavi, S. K. The General Balance in the Six Dimensional of Space-Time. *Preprints* **2023**, 2023081112. https://doi.org/10.20944/preprints202308.1112.v2
8. Mousavi, Seyed Kazem. "Artificial Self-Awareness In Over Time." *Qeios. doi* 10 (2024).https://doi.org/10.32388/YLXN96.2
9. Mousavi, S. K. Information Transfer Based on Brains Entanglement. *Preprints* **2023**, 2023081731. https://doi.org/10.20944/preprints202308.1731.v2
10. https://www.researchgate.net/publication/389855523_The_Nature_of_Time_in_the_Brain_and_Universe